Macromolecules

pubs.acs.org/Macromolecules Article

Microscopic Morphology and Dynamics of Polyampholyte and Cationic Ionomers

Nazanin Sadeghi, Juhyeong Kim, Kevin A. Cavicchi, and Fardin Khabaz*

Cite This: https://doi.org/10.1021/acs.macromol.4c00039 Read Online

ACCESS | Metrics & More | Article Recommendations | Supporting Information

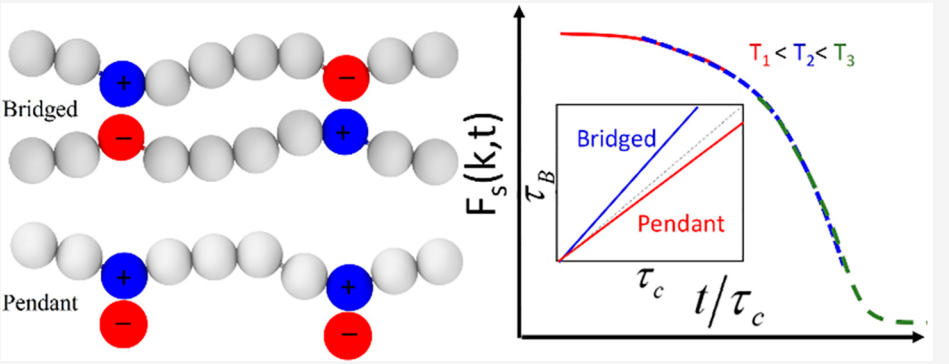

ABSTRACT: Molecular dynamics (MD) simulations are performed using a coarse-grained model of polyampholyte ionomers in which both types of ions are incorporated in the polymer chain and, consequently, the ion-pairs form bridges across the chains (i.e., bridged ion-pair) and compared their dynamics and structures with the conventional cationic ionomers, where only cations are incorporated into the polymer chain (e.g., pendant ion-pair). While the glass transition temperatures of both structures are comparable, mesoscale ordering within large, string-like aggregates is observed in the polyampholyte (bridged) ionomer instead of square-like aggregates in the cationic (pendant) ionomer. Both systems show dynamical heterogeneities at temperatures above T_g, which persist at higher temperatures for the bridged ionomers. A linear correlation between the lifetime of the ionic bonds and the dynamic relaxation time over a wide temperature range is observed. A comparison of these time scales showed that ions have collective dynamics in the bridged ionomers. Furthermore, the intermediate scattering function data obtained at different temperatures can collapse onto master curves, which confirms the applicability of the time−temperature superposition principle in these structures. Overall, this study shows that modifying the chain connectivity of the ion-pairs provides an alternative route to control the morphology and dynamics of ionomers.

I. INTRODUCTION

Ionomers are polymers that contain a small fraction of ions in their backbone,[1−7] and their electrical, thermal, and mechanical properties are governed by a combination of backbone conformation and strength of the electrostatic interactions between ionic groups.[8,9] Ion-pairs can associate to form ionic nanodomains,[10] which behave as multifunctional physical cross-links, thus providing substantial changes in mechanical, optical, dielectric, dynamic, and rheological properties of the polymer chains.[11−13] Among these properties, their ability to tune their rheological and mechanical properties, in which they show solid-like behavior at low temperatures and flow behavior at high temperatures, stems from the degree of nano/microphase aggregation.[14]

A common phenomenon in ionomers is ionic aggregation, which arises from the microphase separation of ions caused by the low dielectric constant of the polymer.[4] This ionic association in the relatively nonpolar polymer matrix has long been recognized as the origin of variations in the properties of ionomers in comparison to their nonionic equivalent.[15] A clear understanding of ionomer structure−property relationships is of great value since several factors, including ion content, chain architecture, type of cation and anion, and thermal and mechanical history, can all affect an ionomer's microstructure.[12]

Morphological investigations on two different ionomer structures in which the anion covalently bonded to the polymer chain either forms a backbone bond or was bonded through a side group display distinct characteristics.[16] The latter exhibited discrete aggregates with a narrow size

Received: January 5, 2024
Revised: April 12, 2024
Accepted: April 17, 2024

https://doi.org/10.1021/acs.macromol.4c00039
Macromolecules XXXX, XXX, XXX−XXX

distribution and a notable liquid-like order between its well-defined aggregates. In contrast, the former showed large percolated ionic aggregates that extended throughout the system, displaying a broad size distribution.[16] Studying the low wave vector peak in X-ray scattering caused by the aggregates (i.e., the ionomer peak),[4] showed that having a large spacing between charged beads on the backbone led to the formation of larger aggregates than those with smaller ones.[17] Morphology of ionomers with precisely distributed side-group bonded ions at elevated temperatures showed that ionic aggregates have liquid-like order and interaggregate distance increased with the overall volume fraction of pendant ions.[18] This distance can be controlled by the spacer length, side chain ionic group volume, and chain architecture.[18] The dependence of the morphology of random ionomers on the fraction of ions and electrostatic interaction strengths was studied by defining a percolation point as the transition of the cluster size distribution from the stretched exponential to power distribution. Below the percolation point, increasing electrostatic interaction resulted in a decrease in the intercluster distance. Conversely, above the percolation point, an increase in electrostatic interaction led to a more densely packed percolated structure with greater spaces between clusters.[19] These results emphasize the significance of the ionic structure architecture, charge distribution, and charge density in determining the morphology of the ionomers.

Incorporating interchain interactions into polymers alters their dynamics.[20−22] The terminal response of ionomer chains relies on the average time an ion pair remains within the ionic cluster, known as the association lifetime, and plays a crucial role in understanding the behavior and dynamics of ionomers.[23] Ion hopping, which is defined as repetitive breaking and reforming of the temporary cross-links, provides the ion transport and ionic relaxation mechanism in ionomers.[24] At relatively low temperatures, the ionic aggregates act as physical cross-links that persist to elevated temperatures, but "ion hopping" of ion pairs from one aggregate to another allows for melt flow. Including a small fraction of ionizable groups on a polystyrene chain, even below the entanglement length, is adequate to slow down the dynamics of the polymer.[25] Two distinct time scales have been identified in ionomers: a fast time scale corresponding to local rearrangements of ions within aggregates and a longer time scale associated with collective rearrangements of ions within a percolated aggregate or between discrete aggregates.[26−28] It has been shown that the diffusion coefficient of ionic groups was about 5 orders of magnitude higher than the diffusion coefficient of the polymer chains, which underscores the essential role of ion hopping in facilitating the rapid movement of cations compared to the center of mass of the polymer chains. Notably, both the terminal relaxation time (representing polymer chain relaxation) and ion-hopping times (reflecting ionic group motion) exhibit similar activation energies, consistent with current theories regarding the dynamics of associating polymers.[29] Alternatively, ions may show a collective rearrangement, which involves two nearby clusters to combine and later break apart and have some ions exchanged while they were together.[26] A detailed study on microscopic dynamics of butyl rubber ionomers showed that the effective lifetime of ion pairs is mainly determined not by the absolute time scale of localized motion of the ions belonging to a cluster, but rather by the factors governing the departure of these groups from the cluster and their subsequent translational motion through the non-polar unpolar matrix.[30]

Another interesting ionomer chain architecture is a polyampholyte, where both anions and cations are covalently bonded to the polymer chain. In the system with both ions covalently bonded to the polymer chains, the ion-pairs form bridges across chain segments, as opposed to a pendant ion-pair with a counterion not covalently bonded to the polymer chain. Salamone et al.[31] first prepared physically cross-linked polyampholyte ionomer networks by free radically copolymerizing styrenic ion-pair comonomers (IPC), where both the anion and cation contain a polymerizable double bond with nonionic comonomers. Recently, Deng and Cavicchi[32] revisited that ionomer structure and synthesized an organic IPC based on styrenic monomers and copolymerized it with *n*-butyl acrylate (BA) using reversible addition−fragmentation chain transfer polymerization to study the role of covalent bonding of the counterion on their viscoelastic properties. Comparison of the structure of this ionomer with chemically similar cationic and anionic ionomers, in which only one type of ion is covalently bonded to the backbone, demonstrated a significant increase in the T_g and the onset temperature of the terminal regime in isochronal temperature sweeps of the bridged structure, which allows the bridged ion pairs to act as long-lived physical cross-links at room temperature. The poor microphase separation between the neutral and ionic segments led to an increase in the effective volume fraction of the ion-rich domains. Consequently, the modulus of the ionomers was enhanced, while the ion-rich domains were simultaneously plasticized by the low T_g BA segments. This plasticization facilitated ion hopping at elevated temperatures, enabling thermoplastic processing at elevated temperatures. Thus, the bridged ionomers have tunable mechanical properties since the strength of physical cross-linking can be controlled. In another research study, Deng et al.[33] synthesized a copolymer of the bridged and pendant ionomers and were able to monotonically tune the T_g by varying the fraction of bridged ion pairs. A molecular-level understanding of phase behavior and ionic dynamics and their dependence on different parameters, such as chain architecture, is required to design the ionomer for the desired application.

In this paper, inspired by the experimental work of Deng and Cavicchi,[32] we investigated the structure and dynamics of a polyampholyte ionomer (i.e., bridged ionomer) and a cationic ionomer (i.e., pendant ionomer) as shown in Figure 1. We were interested in finding answers to the following: (1) How do the microstructure and dynamics of the bridged ionomer differ from the pendant one? (2) What is the effect of temperature on the morphology of these two ionomers? (3) Can we utilize the relaxation times in these ionomers to provide a comprehensive picture of the equilibrium dynamics? To answer these questions, we used MD simulations to understand the morphology and dynamics of bridged and pendant ionomers, and our results are qualitatively consistent with the experiments in that two transition temperatures are seen and the T_g of the bridged ionomer was slightly higher compared to the pendant ionomer. They show different aggregate structures that led to different ionic bond lifetimes. Different dynamics are seen in the two structures. A comparison of the two governing time scales (ionic bond lifetime and dynamical relaxation time) shows that in the bridged ionomers, ions have collective dynamics, unlike the pendant structure in which ion-pair dissociation occurs before

https://doi.org/10.1021/acs.macromol.4c00039
Macromolecules XXXX, XXX, XXX−XXX

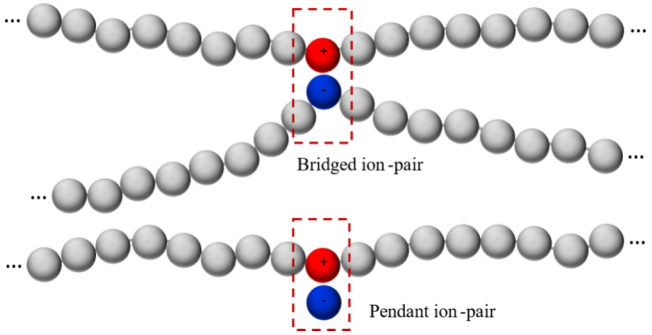

Figure 1. Schematic view of the bridged (top) and pendant (bottom) ionomers. Every charged monomer is precisely placed in the backbone with a spacing length of 9 neutral monomer beads. In the bridged architecture, both the anion and cation are placed in the backbone, and thus, ionic interactions between anions and cations of different chains bridge them together. In the pendant architecture, only the cations are placed in the backbone, while an equal number of anions is present in the system.

escaping the local environment. Overall, our findings in this work underscore the effect of bonding both types of ions to the backbone on governing the association lifetime and in creating a stronger ionic network.

II. SIMULATION DETAILS AND METHODS

II.A. Model, Interaction Potential, and Initial System Preparation. A generic coarse-grained polymer model based on the Kremer–Grest bead–spring framework[34] in MD simulations that include spherical beads attached via finite extensible nonlinear elastic (FENE) spring bonds was used to construct ionomers with two different structures, pendant and bridged. The former is a conventional cationic ionomer, and the latter is a polyampholyte ionomer. Each system consists of 625 chains with a chain length of 40 beads with a mass of m and diameter of σ, in a large cubic box, Figure 1. In the bridged structure, both the anion and cation were bonded to the backbone, whereas in the pendant structure, only cations were bonded to the backbone and an equal number of anions were freely added to the system, as seen in Figure 1. The latter is similar to the "ionene" structure studied by Hall and co-workers.[16,17,26] In both structures, ions are equally spaced throughout the chain with a spacer length of 9 beads. In this model, each neutral polymer bead can approximately be mapped to three CH_2 units in a polyethylene backbone[35]; thus, the average bond length of a FENE bond, 0.96σ, roughly equals the distance covered by three C–C bonds along the backbone,[34] yielding σ = 0.48 nm.[17] The charge distribution on the backbone of both structures corresponds to the extent of gelation of three, considering them as stickers in an associative polymer framework.[36] Dimensionless distance (r), energy (U), temperature (T), and time (t) were determined by scaling them by σ, well-depth of potential energy ε_{LJ},ε_{LJ}/k_B (k_B is the Boltzmann constant),[37] and $\sqrt{\sigma^2 m/\varepsilon_{LJ}}$, respectively. Nonbonded beads interacted through a Lennard-Jones (LJ) potential[38] with a cutoff distance of 2.5, with shifting to zero at the cutoff distance, and adjacent beads were connected by the finitely extensible nonlinear elastic (FENE) potential,[39] respectively:

$$U_{LJ}(r) = \begin{cases} 4[(\frac{1}{r})^{12} - (\frac{1}{r})^{6} - (\frac{1}{r_c})^{12} + (\frac{1}{r_c})^{6}], \text{ for } r_c \le 2.5 \\ 0, \text{ for } r_c > 2.5 \end{cases} \quad (1)$$

$$U_{Bond}(r) = -\frac{K}{2} r_0^2 \ln[1 - (\frac{r}{r_{max}})^2] \quad (2)$$

where r_c is the cutoff distance.[40] In the FENE model, K is set to 30 and r_{max} is the maximum bond length and is set to 1.5.

The ionic interactions were captured by adding Coulomb interaction between two beads with charges q_1 and q_2 according to $U_c(r) = \frac{q_1 q_2}{4\pi\varepsilon_0\varepsilon_r r}$, where ε_r is the dielectric constant of the medium and ε_0 is the vacuum permittivity. In addition, a long-range electrostatic interaction between the charged beads was handled using the particle–particle particle-mesh algorithm.[41] At a constant temperature T, ε_r is inversely proportional to the Bjerrum length,[42,43] $l_B = \frac{e^2}{4\pi\varepsilon_0\varepsilon_r k_B T}$, defined as the distance the Coulomb interaction equals to $k_B T$, where e is the elementary charge. At room temperature, the σ/l_B value corresponds to ε_r = 3.7, which was kept constant. In all simulations, the periodic boundary conditions and a velocity Verlet algorithm with a time step of 0.005 was used in the LAMMPS[44] package. Starting with a large simulation box composed of ionomer chains, an isothermal–isobaric ensemble (i.e., a constant number of atoms, temperature, and temperature, NPT) was used to compress the box at a dimensionless temperature of T = 1 and pressure of P = 1. The pressure was controlled using the Nose–Hoover barostat.[45]

II.B. Quenching Protocol. Pendant and bridged ionomers were quenched from a temperature of T = 1.80 to a low temperature of T = 0.05, in a stepwise fashion with a temperature step size of ΔT = 0.05 (cooling rate = $10^{-6}\sqrt{\varepsilon^3/\sigma^2 m k_b^2}$) in an NPT ensemble at the pressure of P = 0. After equilibration in the NPT ensemble, the dynamics of system was run in a canonical ensemble (i.e., a constant number of atoms, volume, and temperature, NVT) for a duration of 2×10^7steps for generating trajectories. In all simulations, a Nosé–Hoover thermostat was used to control temperature, with a time step of dt = 0.005.[46] Number density was recorded at each temperature and was used to calculate the reduced volume of the ionomers. In this work, we focused on a charge density value of $\hat{q}$ = 0.1, which is defined as the fraction of charged to the neutral beads.

II.C. Dynamics. The mean squared displacement (MSD) $\langle \Delta r^2(t) \rangle$ of anions and cations as a function of time at different temperatures was measured to quantify the dynamics of the ionomer network according to the following relationship:

$$\langle \Delta r^2(t) \rangle = \frac{1}{N_p} \sum_{i=1}^{N} \langle |\mathbf{r}_i(t + t_0) - \mathbf{r}_i(t_0)|^2 \rangle \quad (3)$$

where $\mathbf{r}$ and N_p are the position vector of an anion or cation and the total number of anions or cations, respectively, and t is the time. For performing these calculations, the trajectories of anions and cations were recorded at every 10^4 MD steps at several temperatures in the range of T = 0.3 to 1.5 to characterize the dynamics of ionomers in transition and melt regimes.

III. RESULTS AND DISCUSSION

III.A. Volumetric Data. The reduced volume (V) of the system and thermal expansion coefficient (α) are calculated for both bridged and pendant structures, as seen in Figure 2. At higher temperatures, the pendant ionomer shows a reduced volume higher than that of the bridged one. This can be due to the pendant structure of the ion-pair, which has less constraint on their mobility; hence, there is more free volume available at higher temperatures in that structure compared to the bridged one. We have performed these calculations for systems with higher charge density ($\hat{q}$ = 0.2) and observed the same behavior (Figure S1A).

The glass transition temperature (T_g) is determined by finding the intersection point of the fitted lines in the melt and glassy region of the specific volume-temperature plot (Figure 2A). In order to identify these regimes, we determine the thermal expansion coefficient α using $\alpha = \frac{1}{V}\left(\frac{\partial V}{\partial T}\right)_p$ at different temperatures[47,48] as shown in Figure 2B as a function of

https://doi.org/10.1021/acs.macromol.4c00039
Macromolecules XXXX, XXX, XXX–XXX

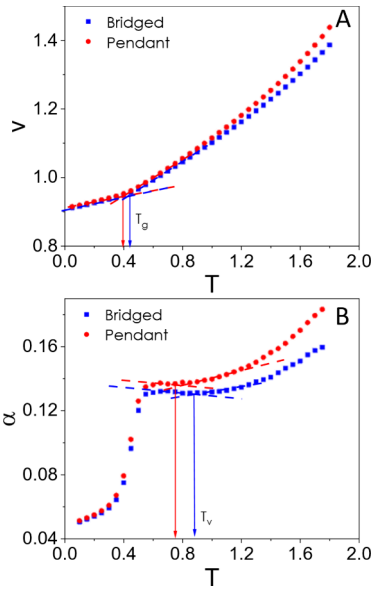

Figure 2. (A) Reduced volume (V) and (B) thermal expansion coefficient (α) of bridged and pendant systems with a charge density of 0.1 as a function of the reduced temperature (T). The second transition temperature, which is reminiscent of the topology freezing temperature in vitrimers, is marked by T_v.

temperature for both structures. In glassy materials, it is common to observe a plateau in α at high temperatures, which is associated with the melt/rubbery regime.[49] Over the transition regime, there is a significant drop in α, which is an indicator of T_g, while in the glassy regime, no plateau is seen, and instead, there is a slight decrease in α with decreasing temperature. The latter corresponds to the nature of glass-forming materials since they are always out of equilibrium.[49,50] The same behavior is seen for the bridged and pendant structures with a charge density of $\hat{q} = 0.2$ (Figure S1B) with a small increase in the T_g of both structures ($T_g \approx 0.5$ and 0.455 for bridged and pendant, respectively). At temperatures well above T_g, α of chemically cross-linked polymers follows the trend seen in glass-forming materials, but in both bridged and pendant ionomers, a significant increase in α is seen, which is more pronounced in the pendant structure. At these temperatures, due to consecutive association/dissociation of ionic cross-links, more free volume is available in the ionomer network than in the permanent cross-linked polymers, leading to an increase in the specific volume. As a result, the thermal expansion coefficient α of the ionomer initially experiences a slight decrease, reaches a minimum, and then begins to rise. A second transition temperature, which is reminiscent of the topology freezing temperature T_v in vitrimers,[51−54] can be identified in these ionomers, as the temperature where the initial decay of α and the subsequent increase intersect (T_v = 0.77 for pendant and T_v = 0.87 for bridged structure). The presence of T_v aligns with experimental observations of similar structures.[32] Above this temperature, the rate of ionic bond association and dissociation or physical bond exchange increases, and therefore the topology of the network changes more frequently and leads to larger free volume than that at lower temperatures.[51,52] The noncovalently bonded counter-ions in the pendant structure enhance the rate of the physical bond exchange at elevated temperatures, and thus, higher values of α (lower T_v) are seen for the pendant structure compared to the bridged structure at high temperatures.

III.B. Morphology. We quantify the local structure of ions using the radial distribution function ($g(r)$) at a steady state, as presented in Figure 3A−F. The first $g(r)$ peak of anion−cation

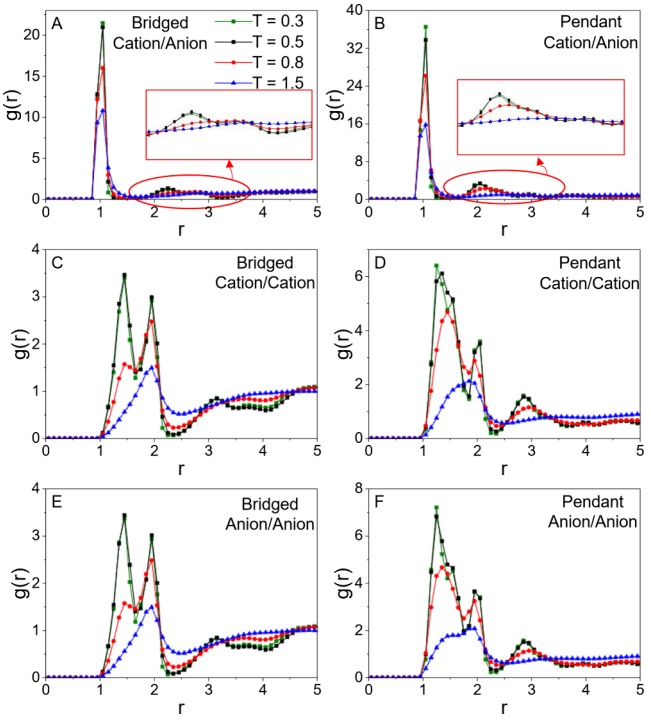

Figure 3. Radial distribution function bridged (left) and pendant (right) structures with a charge density of 0.1 at different temperatures between (top) cation and anion, (middle) cation and cation, and (bottom) anion and anion. The color coding in parts (B)−(F) is the same as in part (A). Insets of (A) and (B) correspond to the zoomed-in $g(r)$ between r = 2 and r = 3.

for both structures is at the distance of 1.05σ, which is nearly the anion−cation association distance, while for cation−cation and anion−anion pairs, these peaks are shifted to a slightly higher distance of 1.3σ. This observation indicates a tighter assembly of the oppositely charged ions than the like ions due to the electrostatic interactions between anions and cations. The presence of a broad peak in the $g(r)$ of anion−cation at the distance of around 2σ corresponds to mesoscale order in both structures. Decreasing the temperature intensifies the height of the first peak of the $g(r)$ in both structures, indicating that at lower temperatures, ionic clusters are packed tighter than at high temperatures. By increasing temperature, the second peak in the $g(r)$ of the anion and cation fades away, showing that there is no long-range structuring at high temperatures. The intensity and position of the second peak in the $g(r)$ of the cation−anion in the bridged and pendant structures have been depicted in Figure S2.

There is also a second peak in the $g(r)$ of cation−cation and anion−anion in both structures, which is more significant for the pendant ionomer, at a distance two times the distance of the first peak in the anion−cation. This peak merges into one broad peak at a distance of 1.95σ with increasing temperature. This indicates further structuring between like ions. Also, in the $g(r)$ of the cation−cation and anion−anion in the pendant structure, a third small peak can be seen at the distance of 2.85σ, which fades away by increasing temperature, indicating that pendant clusters break down, as in the bridged structure.

https://doi.org/10.1021/acs.macromol.4c00039
Macromolecules XXXX, XXX, XXX−XXX

These results align with the structure factor data, which are determined from the Fourier transform of the radial distribution function and presented in Figure S3. The pendant structure shows a more intense ionomer peak at the low wavevector, and the peak in the bridged structure is broader and less intense at larger wavevectors than the pendant one. The latter corresponds to the long-range order in the percolated ionic network of bridged structure.

The potential mean force (PMF), which corresponds to Helmholtz free energy, of bringing two ions from infinite distances into a cluster has been calculated using the following equation[55]:

$$W(r) = -k_B T \ln g(r) \tag{4}$$

The results of this free energy calculation for various temperatures can be seen in Figure 4. The PMF curves show

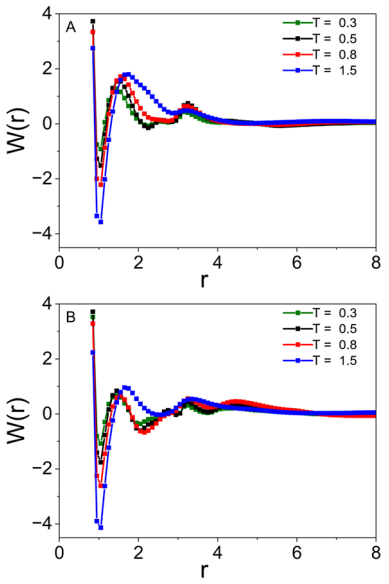

Figure 4. Potential mean force (PMF) of the (A) bridged and (B) pendant ionomers at different temperatures.

the presence of one or two minima at the association point of ion pairs as well as a shallow third minimum at longer distances, which corresponds to a second neighboring shell in an ionic cluster. By increasing temperature, the depth of the minimum for the ion pair association increases. To demonstrate the contributions of internal and entropic energies to cluster formation, we can use the following equation:

$$W(r) - W(\infty) \equiv \Delta F = \Delta U - T\Delta S \tag{5}$$

where $W(\infty) = 0$ and $\Delta S = -\frac{\partial W(r)}{\partial T}$. Thus, energetic and entropic contributions to the free energy of clustering can be determined (Figure S4). These contributions are negative close to the first minimum point, thus both promoting the ion pair formation. However, close to the second minimum, the energetic part of the free energy is the main driving force of ionic association, and similarly, at larger distances, the entropic contribution is more dominant.

Both ionomers form ionic aggregates but with different shapes at different temperatures (Figure 5A). At low temperatures, the bridged ionomer forms a string-like percolated network that spans throughout the simulation box, but the pendant one shows bulky strings with a square-like arrangement of ions (see Figure S5). In both structures, the aggregates break into smaller clusters by increasing temperature. To gain a better understanding of the morphology, cluster analysis is conducted on both bridged and pendant ionomers. Snapshots of the clustering in both structures at three temperatures are presented in Figure 5B (each color corresponds to a unique cluster). In this analysis, we presume that ions belong to one cluster if they are in the vicinity of 1.2σ, which is slightly higher than the diameter of each particle (Figure 5C). At high temperatures, there is a slightly higher number of clusters in the bridged ionomer than the pendant one, but these aggregates are smaller in size, based on the radius of gyration (R_g) of the largest cluster at each temperature in Figure 5D. The latter is also evident from snapshots of cluster analysis of both ionomers at $T = 1.5$. Except for $T = 0.8$, the pendant ionomer shows a slightly larger size for the largest cluster (Figure 5D). Higher uncertainties in the mean R_g of the largest clusters at temperatures around unity are due to high thermal fluctuations in the systems that cause the continuous breaking and reforming of the largest cluster. At temperatures above this limit, the ions are dissociated, and thus, the size of the largest cluster has a small error bar. Relative anisotropy (κ^2) of the clusters (Figure 5E), which varies from 0 for spheres to 1 for straight rods, is calculated using the following equation[56,57]:

$$\kappa^2 = 1 - 3\frac{\lambda_1\lambda_2 + \lambda_2\lambda_3 + \lambda_3\lambda_1}{(\lambda_1 + \lambda_2 + \lambda_3)^2} \tag{6}$$

where λ_1, λ_2, and λ_3 are eigenvalues of the gyration tensor for a given cluster. The average cluster shape anisotropy for the largest cluster is smaller for the bridged ionomers at low temperatures, indicating an isotropic arrangement, while at higher temperatures, both structures have nearly the same κ^2 values, $\kappa^2 = 0.5$ and 0.37 for bridged and pendant structures at $T = 1.5$, respectively. These κ^2 values show that bridged structures form more elongated clusters, while in the pendant ionomer, relatively large isotropic aggregates are formed at higher temperatures. The uncertainties in calculating κ^2 are high due to thermal fluctuations, which promote continuous breaking and reforming of the largest cluster at a temperature around unity, and thus, the cluster shape changes frequently. Above this limit, dissociation of the ions occurs, and the size and shape of the ion clusters become uniform. The average size distribution of the clusters as a function of temperature is plotted in Figure 6, and in both cases, the distribution shows bimodal behavior, which vanishes at higher temperatures. At $T = 0.6$, for the pendant ionomer the highest distribution probability is seen for larger R_g values, unlike the bridged ionomer in which smaller R_g values are the most probable. This observation indicates that the bridged ionomer forms small, percolated aggregates, whereas in the pendant structure, larger isolated clusters have been formed at low temperatures. The peak of the distribution of cluster sizes shifts to small values in both structures by increasing temperature, indicating that at sufficiently high temperatures aggregates in both structures break into small clusters.

III.C. Dynamics. We computed the MSD of anions and cations at different temperatures to quantify the dynamics of the ionomers in Figure 7. At $T = 0.3$, both ionomers are in a glassy regime, and ions do not show significant movement; thus, both bridged and pendant ionomers show identical MSD

https://doi.org/10.1021/acs.macromol.4c00039
Macromolecules XXXX, XXX, XXX−XXX

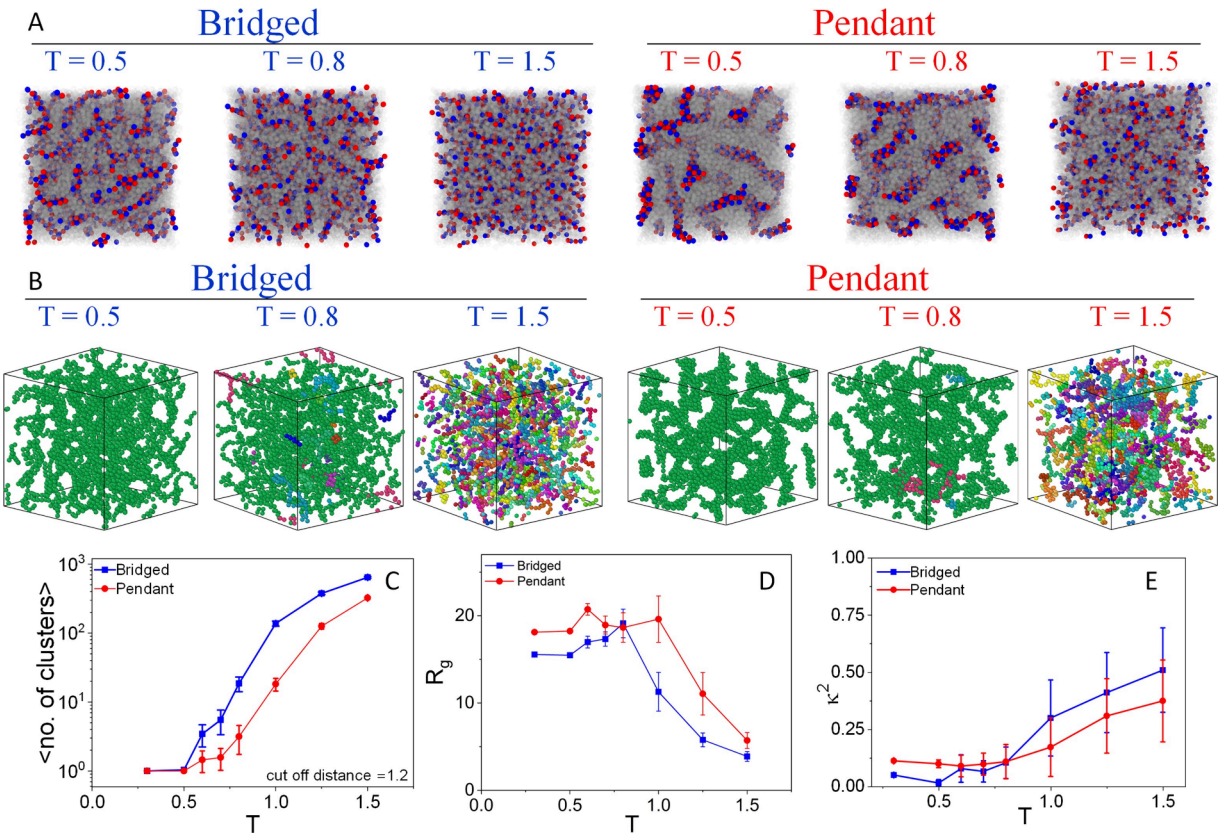

Figure 5. (A) Snapshots of the simulation box of the bridged and pendant ionomers at reduced temperatures of 0.5, 0.8, and 1.5. (B) Cluster analysis of bridged and pendant structures in two different temperatures and with a charge density of 0.1. Each color represents a unique cluster. (C) Average number of clusters in the bridged and pendant ionomers, (D) radius of gyration (R_g), and (E) relative anisotropy of the largest cluster as a function of the temperature.

values. As the temperature increases, at about T = 0.8, both structures start to approach the diffusive regime, and at T = 1, all MSD curves show a slope close to unity. Slopes of the MSD curves of the nonionic beads of bridged and pendant ionomers as a function of observation time have been plotted in Figure S6. Since anions in the pendant ionomer are not covalently bonded to the backbone, they have more freedom in movement and show a higher MSD at higher temperatures than in the bridged ionomer. On the other hand, cations show similar behavior in both structures at low to moderate temperatures, but at the highest temperature, cations in the pendant structure are more mobile than the cations in the bridged structure. This observation indicates that the presence of physical cross-links between ions creates a temporary network that slows the diffusion and mobility of the whole chain, and since the anions of the pendant structure are not covalently bonded to the chain and have less constraint on their movement, there is a minor enhancement of mobility in the pendant structure compared to the bridged one.

The characteristic relaxation time of a 40-bead chain can be calculated using sticky Rouse time, τ_R^s, which is the time that a polymer chain diffuses a distance of its size. Using the MSD of nonionic beads and considering the radius of gyration as the size of the polymer chain, this relaxation time, which is close to the terminal relaxation time of the system, is approximated. As can be seen in Figure 7, the sticky Rouse time of the bridged ionomer melt is one order of magnitude higher than the corresponding time scale in the pendant ionomer, which is an indication of the delayed dynamics due to the presence of a more robust ionic network than the pendant one.

The individual square of displacement of anions and cations in the pendant ionomers, Δr_i^2, as a function of observation time, is plotted in Figure 8, along with their corresponding MSD. As can be seen from the figure, there is a broader distribution in the displacement of ions at long times, indicating the different dynamics of individual chains. This behavior suggests that the dynamics of ions in these ionomers may show heterogeneous behavior.

We calculate the self-part of the van Hove autocorrelation function, $G_s(r, \Delta t)$, which for a given particle determines the probability of traveling distance of r over time interval t, for both types of ionomers in short and long times at various temperatures (Figure 9) to observe the distribution of dynamics, using the following equation[58]:

$$G_s(\mathbf{r}, \Delta t) = \frac{1}{N} \sum_i \delta(\mathbf{r} - |\mathbf{r}_i(t + \Delta t) - \mathbf{r}_i(t)|) \tag{7}$$

where N is the number of ions and δ is the Dirac delta function. If ions follow a Fickian diffusive motion, then the behavior of the $G_s(r, \Delta t)$ can be approximated by a Gaussian function based on $G_s^g(r, \Delta t)$, which is given as $G_s^g(r, \Delta t) = \left(\frac{3}{2\pi\langle\Delta r^2\rangle}\right)^{3/2} \exp\left(-\frac{3r^2}{2\langle\Delta r^2\rangle}\right)$.[59] Results show that at low temperatures, below and close to T_g, the van Hove functions show a substantial deviation from a Gaussian behavior by showing an exponential tail and crossover between

https://doi.org/10.1021/acs.macromol.4c00039
Macromolecules XXXX, XXX, XXX−XXX

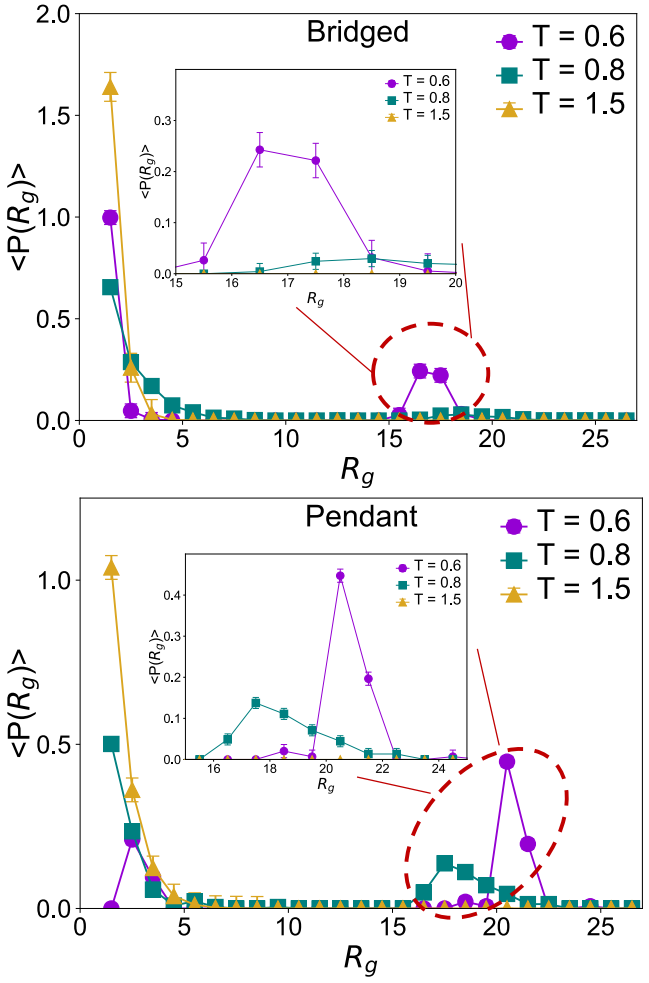

Figure 6. Average probability distribution of the radius of gyration (R_g) of the (A) bridged and (B) pendant ionomers at various temperatures.

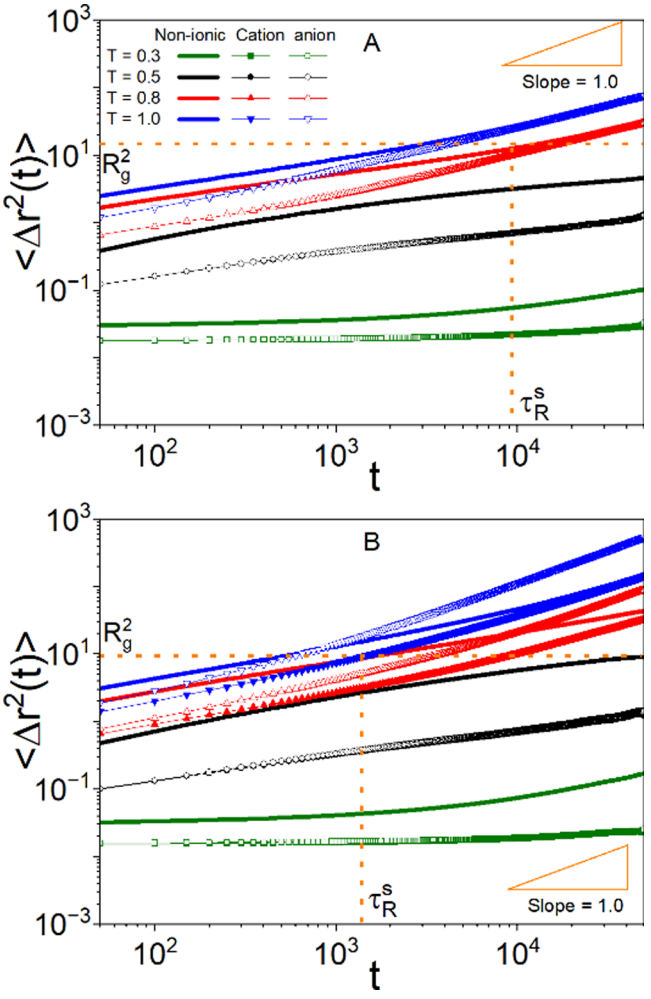

Figure 7. Comparison of the MSDs of cations, anions, and neutral beads of (A) bridged and (B) pendent ionomers at different temperatures.

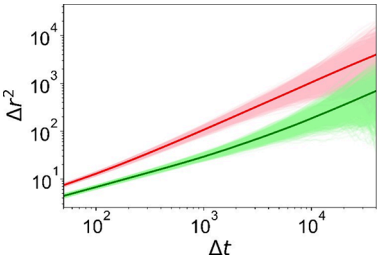

Figure 8. Square of displacement of anions (red) and cations (green) in the pendant ionomers at the temperature of T = 1.5. The bold line is the average MSD.

the Gaussian prediction, which is an indicator of dynamical heterogeneities in both bridged and pendant structures.[58] At temperatures higher than T_g, the variations in the van Hove function show that anions in the pendant structure can move larger distances since they are not covalently bonded to the backbone, but even cations in the pendant structure show slightly larger displacement than cations in the bridged structure at long times. The latter indicates that anions facilitate movement of the chains in the pendant structure. At higher temperatures, $G_s(r, \Delta t)$ shows a closer behavior to a Gaussian distribution since the motion of ions is more likely diffusive, and dynamical heterogeneities have a minor effect on the overall dynamics. At long times, dynamical heterogeneities are still noticeable at low and moderate temperatures for both ionomers but vanish at high temperatures for the pendant ionomers. However, even at temperatures as high as T = 1 dynamical heterogeneities can be seen at $\Delta t = 10^4$ in the bridged ionomer.

To better understand the role of the dynamics of physical cross-links formed by the electrostatic interactions between ions, we calculate their association lifetime using the decay of the bond autocorrelation function defined as

$$C(t) = \frac{\langle H(t + t_0)H(t_0)\rangle}{\langle H(t_0)^2\rangle} \quad (8)$$

where $H(t)$ is a binary function.[51] If a pair of ions are connected at a vicinity of r = 1.2 from each other, over a time interval of t, then $H(t)$ = 1, otherwise $H(t)$ = 0. The values of this correlation function, which is representative of the ionic bonds lifetime, are shown in Figure S7 as a function of time and for various temperatures. At temperatures lower than T_g since there is no significant movement, $C(t)$ does not decay and shows values close to unity, which shows that there is no significant change in the connectivity of the ions over time. As the temperature increases, $C(t)$ decays and shows a fast drop. This behavior of $C(t)$ is best described by fitting the data to a

https://doi.org/10.1021/acs.macromol.4c00039
Macromolecules XXXX, XXX, XXX−XXX

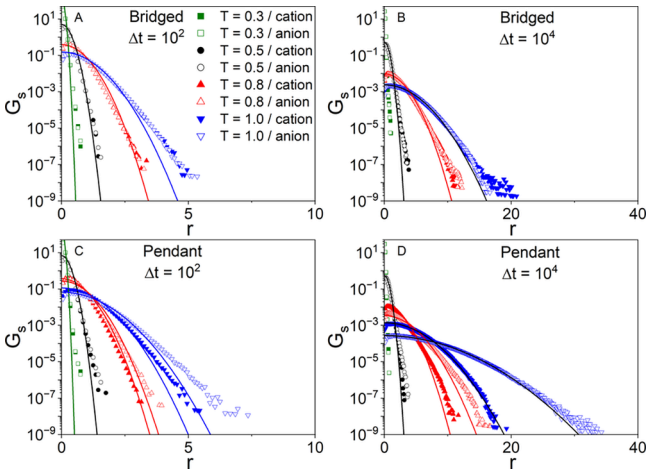

Figure 9. Van Hove function $G_s(r, t)$ of anions and cations in bridged (top) and pendant (bottom) structures at short times ($\Delta t = 10^2$ − left panel) and long times ($\Delta t = 10^4$ − right panel). The lines represent the Gaussian predictions for the van Hove function.

stretched exponential function in the form of $C(t) = \exp(-(t/\tau)^{\beta})$, where β is the stretching exponent and τ is the relaxation time. The values of β for the bridged and pendant structures are shown in Figure S8 and are around 0.5 for both structures. The effective lifetime of ionic bonds, which is the time needed for a single ion pair to separate from each other, is then determined using $\tau_B \equiv \int_0^\infty C(t)dt = \frac{\tau}{\beta}\Gamma(\frac{1}{\beta})$, where Γ is the Gamma function.[60] The values of τ_B as a function of the inverse temperature for both bridged and pendant structures are shown in Figure 10 and have been compared to the sticky

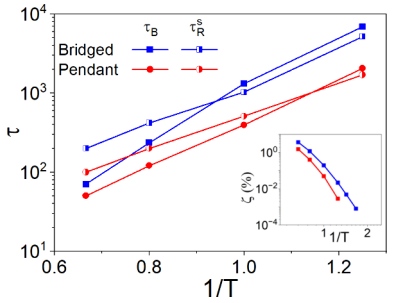

Figure 10. Sticky relaxation time (τ_R^s) and ion-pair lifetime (τ_B) of the bridged and pendant ionomers as a function of the inverse temperature. Inset: dissociation fraction (ζ) as a function of the reciprocal of temperature for the bridged and pendant ionomers.

relaxation time of the ionomers. Both time scales are consistently larger for the bridged structure. Also, the crossover between τ_B and τ_R^s is happening at higher temperatures in the bridged ionomer compared to the pendant structure, which can be an indication of stronger ionic network in the bridged ionomer. τ_B in both structures shows a deviation from the Arrhenius-like temperature dependence. In the inset of Figure 10, the percentage of isolated ions (ζ), which is called the dissociation fraction, has been plotted as a function of the inverse temperature. The dissociation fraction for both structures increases with an increase in temperature. ζ is about 5% at the highest temperature, which is beyond the second transition temperature for both networks and then sharply decreases to small values by a decrease in temperature. Thus, the latter confirms that the majority of ions participate in network formation in both bridged and pendant ionomers. We also note that this fraction is slightly higher for the bridged ionomer than the pendant one since, in the bridged structure, both ions are bonded to the backbone, and they experience more hindrance in finding an unbonded partner than those pairs in the pendant ionomer. It must be noted that in the bridged structure, the majority of the ionic bonds are intermolecular and only about 10% of bonds are bridging the same chain (Figure S9).

We compute the incoherent intermediate scattering function (ISF), which describes the self- (or tagged particle) dynamics in Fourier space via the spatial wave vector ($\mathbf{k}$)-dependent correlation function to examine the influence of ionic interactions on the dynamics of ionomers:

$$F_s(\mathbf{k}, t) = \frac{1}{N} < \sum_{j=1}^{N} \exp[i\mathbf{k}.\ (\mathbf{r}_j(t) - \mathbf{r}_j(t_0))] > \quad (9)$$

The ISFs are computed at different temperatures and at a wave vector amplitude $|k| = 1$, which corresponds to the location of the first peak in the scattering function. The characteristic time of decorrelation of ISF, τ_c, is then determined by fitting a stretched exponential function to ISF data according to $\tau_c = \frac{\tau}{\beta}\Gamma\left(\frac{1}{\beta}\right)$. At each temperature, fitting this stretched exponential function to ISF data gives access to τ_c, which is the microscopic time that each ion needs to escape from its local environment. The value of β for the bridged and pendant structures decreased from 0.6 to 0.4, by increasing temperature. Figure 11 shows the time dependence of the ISF for the bridged and pendant ionomers and their corresponding relaxation times. The structural relaxation slows down drastically upon cooling. At low temperatures (slightly above T_g), curves in Figure 11A,B show a plateau at short times, which reflects the arrested dynamics of the ions. At long times, all curves decay to values close to zero since the association and dissociation of ionic bonds allow cage rearrangements with a characteristic time τ_c. As can be seen from Figure 11C, the dynamics of ions in both structures exhibits a deviation from Arrhenius-like relaxation. The bridged ionomer showed a slightly larger relaxation time at higher temperatures, while at lower temperatures, cations of the pendant ionomer had a larger relaxation time. Anions of the pendant ionomer show a smaller τ_c than that of the bridged ionomer at all temperatures.

A direct comparison of the relaxation time of ionic bonds (τ_B) with the dynamical relaxation time (τ_c) is established in Figure 12. Results show that these two time scales are correlated with each other over the whole range of temperatures. In the bridged ionomer, $\tau_B = 0.44\tau_c^{1.13}$ and $\tau_B \geq \tau_c$, which show that ions mostly have a collective dynamic and maintain their ionic bond while escaping the surrounding cluster in the bridged structure. On the other hand, $\tau_B = 0.62\tau_c^{1.00}$ and $\tau_c \geq \tau_B$ in the pendant ionomer, which suggests that an ionic bond dissociation occurs before the ion-pair escapes its cluster. These results indicate that the bridged structure can result in an ionomer with a longer-lived physical cross-linking network compared to the pendant ionomer with the same electrostatic strength.

Inspired by our recent work on the dynamics of vitrimers,[52] the ISF data as a function of rescaled time, which is defined as t/τ_c, is plotted in Figure 13. As seen from the figure, the ISFs of bridged and pendant ionomers collapsed perfectly onto a

https://doi.org/10.1021/acs.macromol.4c00039
Macromolecules XXXX, XXX, XXX−XXX

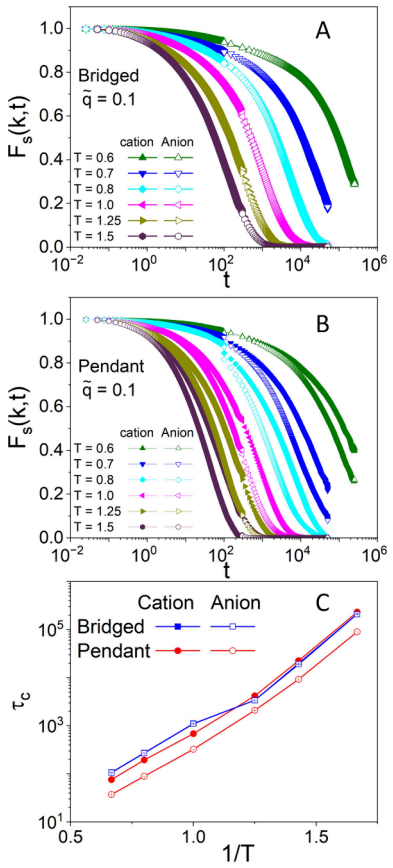

Figure 11. Intermediate scattering function of cation and anion in (A) bridged and (B) pendant ionomers at different temperatures. (C) Dynamical relaxation time of the bridged and pendant ionomers is a function of the reciprocal of temperature.

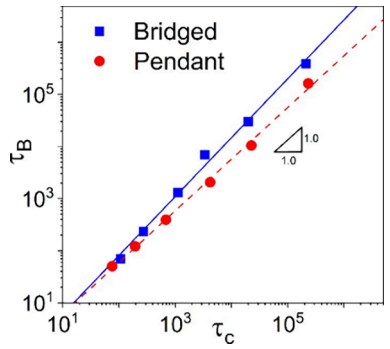

Figure 12. Comparison of the bond lifetime (τ_B) and dynamic relaxation time (τ_c) of the bridged and pendant ionomers.

master curve. At high temperatures, the ISFs reach zero at long times since the association−dissociation of ionic bonds allows the cage rearrangements with a characteristic time τ_c. Similar master curves can be constructed using the dynamical relaxation time of the center of the mass of the ionomer chains or nonionic beads (Figures S10 and S11). This implies that the universality of τ_c enables us to create these master curves.[52] The collapse of ISF data also implies the applicability of the time−temperature superposition (TTS) principle in these systems since one dominant mode of relaxation governs their dynamics. Introducing any anomaly into the structure that may result in the distinct time dependence of ionic association lifetime and dynamics of the network may lead to

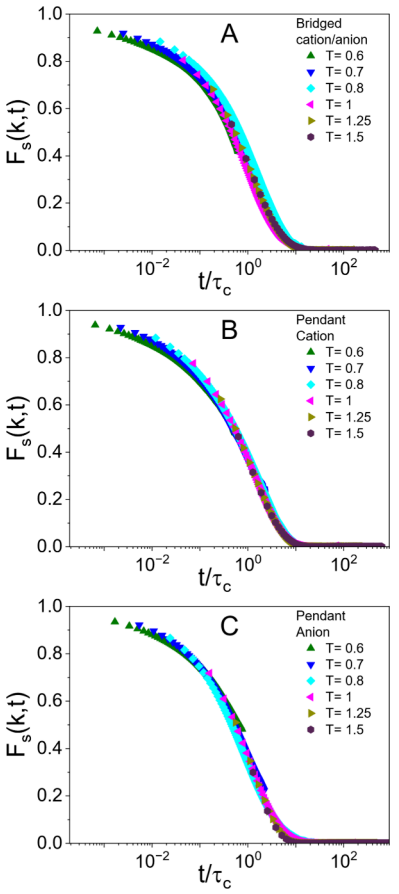

Figure 13. Intermediate scattering function (ISF) of the (A) bridged structure, (B) cations of the pendant structure, and (C) anions of the pendant structure as a function of rescaled time.

the failure of TTS. In this regard, Weiss and Yu showed that TTS is applicable to collapse the linear viscoelastic behavior of sulfonated polystyrene ionomers over 20 decades of frequency, which was in line with earlier findings.[24] Even though TTS is generally expected to fail for phase-separated materials,[61] since multiple relaxation processes for ionic and nonionic domains do not overlap and are widely separated in time in these ionomers, an individual isothermal measurement is not able to access both time scales at a single temperature.[61] Another study on imidazolium-based ionomers with different counterions and side chain lengths showed that TTS can be utilized to construct master curves for those materials since they all showed WLF-type temperature dependence with the same activation energy.[62] On the other hand, TTS fails for telechelic and pendant ionomers of polydimethylsiloxane (PDMS) due to strong differences in the temperature dependence of segmental and terminal relaxation times.[63] In general, the TTS failure is possible if the associative networks are below or at the onset of gelation,[64] which is not the case in our study since the extent of gelation of these ionomers is well above unity.

IV. SUMMARY AND CONCLUSIONS

We performed MD simulations using a bead spring model on two ionomer structures and studied their morphology and dynamics at equilibrium. The bridged ionomers with a cation and anion bonded to the backbone showed slightly higher T_g than the pendant ionomer in which only cations are

https://doi.org/10.1021/acs.macromol.4c00039
Macromolecules XXXX, XXX, XXX−XXX

incorporated in the chain. A second transition temperature, which is similar to the topology freezing temperature in vitrimers was identified in these ionomers,[51−54] Above which the rate of ionic bond association and dissociation (i.e., physical bond exchange) increases, and as a consequence, the topology of the network changes more frequently.

Analysis of morphology revealed that both structures show a tighter assembly of oppositely charged ions due to the electrostatic interactions between anions and cations. The presence of a broad, long-ranged peak in the $g(r)$ of anion−cation pairs at an approximate distance of 2σ, particularly pronounced in the pendant structure, indicates the existence of a mesoscale order in both ionomer structures. This order can either be attributed to large, string-like aggregates in the bridged ionomer or square-like aggregates present in the pendant ionomer. Additionally, the pendant and bridged ionomers exhibited a second peak in the $g(r)$ of the same-charge ions, which merged into a single broad peak, which is more prominent in the pendant structure, by increasing the temperature. The structure factor of the charged beads in both structures displayed a shift to higher temperatures in the bridged structure, indicating long-range order in the percolated ionic network of the bridged ionomer.

The result of quantifying dynamics using MSD calculation revealed that the presence of noncovalently bonded counterions in the pendant structure affects the movement of the entire system at high temperatures. The bridged structure was shown to be able to preserve its ionic network at higher temperatures since there was evidence of dynamical heterogeneities at T = 1.5 in this structure. The two important characteristic time scales that describe the dynamics were the bond association lifetime (τ_B) and the dynamical relaxation time (τ_c). We showed that the ionic bonds in the bridged structure have a longer lifetime than those in the pendant ionomer despite having the same electrostatic interaction strength. This finding underscores the influence of bonding ions on the backbone in controlling the bond association lifetime and establishing a stronger network. Interestingly, we observed a linear correlation between τ_B and τ_c over a wide temperature range. A comparison of these two time scales showed that ions in the bridged ionomer have a collective dynamic and maintain their ionic bond while escaping the surrounding cluster. In contrast, in the pendant ionomer, a series of ionic bond dissociations occurs before an ion escapes its cluster. These results indicate a longer-lived physical cross-linking network in the bridged ionomer than the pendant ionomer with the same electrostatic strength. Additionally, by using τ_c as a rescaling time, we collapsed ISF data obtained at different temperatures into a master curve. The latter implies the applicability of the TTS principle in these ionomers above the gel point. Results provided in this work show that having both ions on the backbone of the chains can lead to a measurable change in the dynamics and morphology. This finding opens new avenues for research to look at the effect of the distribution of these charges on the rheological and mechanical properties of ionomers.

■ ASSOCIATED CONTENT

Supporting Information

The Supporting Information is available free of charge at https://pubs.acs.org/doi/10.1021/acs.macromol.4c00039.

Reduced volume and thermal expansion coefficient of bridged and pendant systems with a charge density of 0.2 as a function of the reduced temperature (T), intensity of the second peak in the $g(r)$ of the anion/cation in the bridged and pendant ionomers as a function of temperature, structure factor of the bridged and pendant structures with a charge density of 0.1 and 0.2 at T = 0.5, PMF and the energetic and entropic contributions as a function of the distance at T = 0.8 for the bridged and pendant ionomer, schematic of arrangement of ions in the bridged and pendant structure based on the average number of the bonds and dissociation fraction, slope of the MSD plot of nonionic beads for bridged and pendant structures as a function of observation time, number of ionic bonds as a function of temperature for the bridged and pendant ionomer, stretching exponent of the bridged and pendant ionomers as a function of inverse temperature, fraction of bridged chains formed intramolecular bonds between anions and cations, ISF of bridged and pendant structure center of mass as a function of rescaled time, ISF of nonionic beads of bridged and pendant structure as a function of rescaled time, dynamic relaxation time of the nonionic beads of bridged and pendant structures as a function of temperature, stretched exponent of the anions and cations in the bridged and pendant ionomers as a function of inverse temperature, normalized van Hove function of anions and cations in bridged and pendant structures at short and long times (PDF)

■ AUTHOR INFORMATION

Corresponding Author

Fardin Khabaz − *School of Polymer Science and Polymer Engineering, The University of Akron, Akron, Ohio 44325, United States; Department of Chemical, Biomolecular, and Corrosion Engineering, The University of Akron, Akron, Ohio 44325, United States;* orcid.org/0000-0002-6879-8587; Phone: (330) 972-5410; Email: fkhabaz@uakron.edu

Authors

Nazanin Sadeghi − *School of Polymer Science and Polymer Engineering, The University of Akron, Akron, Ohio 44325, United States*

Juhyeong Kim − *Department of Physics, The College of Wooster, Wooster, Ohio 44691, United States*

Kevin A. Cavicchi − *School of Polymer Science and Polymer Engineering, The University of Akron, Akron, Ohio 44325, United States;* orcid.org/0000-0002-6267-7899

Complete contact information is available at: https://pubs.acs.org/10.1021/acs.macromol.4c00039

Notes

The authors declare no competing financial interest.

■ ACKNOWLEDGMENTS

J.K. was supported as an REU student by the US National Science Foundation, grant number 2051052.

■ REFERENCES

(1) Eisenberg, A. Clustering of ions in organic polymers. *A theoretical approach. Macromolecules* **1970**, *3* (2), 147−154.

(2) Peiffer, D.; Weiss, R.; Lundberg, R. Microphase separation in sulfonated polystyrene ionomers. *J. Polym. Sci., Part B: Polym. Phys.* **1982**, *20* (8), 1503−1509.
(3) Eisenberg, A.; Hird, B.; Moore, R. A new multiplet-cluster model for the morphology of random ionomers. *Macromolecules* **1990**, *23* (18), 4098−4107.
(4) Eisenberg, A.; Kim, J.-S. *Introduction to ionomers*. Wiley: 1998.
(5) Kirkmeyer, B. P.; Weiss, R. A.; Winey, K. I. Spherical and vesicular ionic aggregates in Zn-neutralized sulfonated polystyrene ionomers. *J. Polym. Sci., Part B: Polym. Phys.* **2001**, *39* (5), 477−483.
(6) Tant, M. R.; Mauritz, K. A.; Wilkes, G. L. *Ionomers: synthesis, structure, properties and applications*. Blackie Academic & Professional: 1997.
(7) Vijayaraghavan, P.; Brown, J. R.; Hall, L. M. Modeling the Effect of Polymer Composition on Ionic Aggregation in Poly(propylene glycol)-Based Ionenes. *Macromol. Chem. Phys.* **2016**, *217* (8), 930−939.
(8) Eisenberg, A.; Rinaudo, M. Polyelectrolytes and ionomers. *Polym. Bull.* **1990**, *24*, 671.
(9) Sing, C. E.; Zwanikken, J. W.; de la Cruz, M. O. Electrostatic control of block copolymer morphology. *Nat. Mater.* **2014**, *13* (7), 694−698.
(10) Yarusso, D. J.; Cooper, S. L. Microstructure of ionomers: interpretation of small-angle x-ray scattering data. *Macromolecules* **1983**, *16* (12), 1871−1880.
(11) Zhang, L.; Brostowitz, N. R.; Cavicchi, K. A.; Weiss, R. Perspective: Ionomer research and applications. *Macromol. React. Eng.* **2014**, *8* (2), 81−99.
(12) Ding, Y. S.; Register, R. A.; Yang, C.-z.; Cooper, S. L. Synthesis and characterization of sulphonated polyurethane ionomers based on toluene diisocyanate. *Polymer* **1989**, *30* (7), 1204−1212.
(13) Wakabayashi, K.; Register, R. A. Morphological origin of the multistep relaxation behavior in semicrystalline ethylene/methacrylic acid ionomers. *Macromolecules* **2006**, *39* (3), 1079−1086.
(14) Sampath, J.; Hall, L. M. Effect of Neutralization on the Structure and Dynamics of Model Ionomer Melts. *Macromolecules* **2018**, *51* (2), 626−637.
(15) Register, R. A. Morphology and structure−property relationships in random ionomers: Two foundational articles from macromolecules. *ACS Publications* **2020**, *53*, 1523−1526.
(16) Hall, L. M.; Stevens, M. J.; Frischknecht, A. L. Effect of polymer architecture and ionic aggregation on the scattering peak in model ionomers. *Phys. Rev. Lett.* **2011**, *106* (12), No. 127801.
(17) Hall, L. M.; Seitz, M. E.; Winey, K. I.; Opper, K. L.; Wagener, K. B.; Stevens, M. J.; Frischknecht, A. L. Ionic aggregate structure in ionomer melts: effect of molecular architecture on aggregates and the ionomer peak. *J. Am. Chem. Soc.* **2012**, *134* (1), 574−587.
(18) Buitrago, C. F.; Alam, T. M.; Opper, K. L.; Aitken, B. S.; Wagener, K. B.; Winey, K. I. Morphological trends in precise acid-and ion-containing polyethylenes at elevated temperature. *Macromolecules* **2013**, *46* (22), 8995−9002.
(19) Ma, B.; Nguyen, T. D.; Pryamitsyn, V. A.; Olvera de la Cruz, M. Ionic correlations in random ionomers. *ACS Nano* **2018**, *12* (3), 2311−2318.
(20) Zhang, Z.; Chen, Q.; Colby, R. H. Dynamics of associative polymers. *Soft Matter* **2018**, *14* (16), 2961−2977.
(21) Rubinstein, M.; Semenov, A. N. Dynamics of entangled solutions of associating polymers. *Macromolecules* **2001**, *34* (4), 1058−1068.
(22) Rubinstein, M.; Dobrynin, A. V. Solutions of associative polymers. *Trends Polym. Sci.* **1997**, *5* (6), 181−186.
(23) Chen, Q.; Tudryn, G. J.; Colby, R. H. Ionomer dynamics and the sticky Rouse model. *J. Rheol.* **2013**, *57* (5), 1441−1462.
(24) Weiss, R.; Fitzgerald, J.; Kim, D. Viscoelastic behavior of lightly sulfonated polystyrene ionomers. *Macromolecules* **1991**, *24* (5), 1071−1076.
(25) Weiss, R. A.; Zhao, H. Rheological behavior of oligomeric ionomers. *J. Rheol.* **2009**, *53* (1), 191−213.
(26) Hall, L. M.; Stevens, M. J.; Frischknecht, A. L. Dynamics of model ionomer melts of various architectures. *Macromolecules* **2012**, *45* (19), 8097−8108.
(27) Frischknecht, A. L.; Paren, B. A.; Middleton, L. R.; Koski, J. P.; Tarver, J. D.; Tyagi, M.; Soles, C. L.; Winey, K. I. Chain and ion dynamics in precise polyethylene ionomers. *Macromolecules* **2019**, *52* (20), 7939−7950.
(28) Agrawal, A.; Perahia, D.; Grest, G. S. Cluster morphology-polymer dynamics correlations in sulfonated polystyrene melts: computational study. *Phys. Rev. Lett.* **2016**, *116* (15), No. 158001.
(29) Tierney, N. K.; Register, R. A. Ion hopping in ethylene−methacrylic acid ionomer melts as probed by rheometry and cation diffusion measurements. *Macromolecules* **2002**, *35* (6), 2358−2364.
(30) Mordvinkin, A.; Suckow, M.; Böhme, F.; Colby, R. H.; Creton, C.; Saalwächter, K. Hierarchical sticker and sticky chain dynamics in self-healing butyl rubber ionomers. *Macromolecules* **2019**, *52* (11), 4169−4184.
(31) Salamone, J.; Tsai, C.; Olson, A.; Watterson, A. Ampholytic polystyrene ionomers from cationic−anionic monomer pairs. *Journal of Polymer Science: Polymer Chemistry Edition* **1980**, *18* (10), 2983−2992.
(32) Deng, G.; Cavicchi, K. A. Tuning the Viscoelastic Properties of Poly (n-butyl acrylate) Ionomer Networks through the Use of Ion-Pair Comonomers. *Macromolecules* **2017**, *50* (23), 9473−9481.
(33) Deng, G.; Schoch, T. D.; Cavicchi, K. A. Systematic Modification of the Glass Transition Temperature of Ion-Pair Comonomer Based Polyelectrolytes and Ionomers by Copolymerization with a Chemically Similar Cationic Monomer. *Gels* **2021**, *7* (2), 45.
(34) Kremer, K.; Grest, G. S. Dynamics of entangled linear polymer melts: A molecular-dynamics simulation. *J. Chem. Phys.* **1990**, *92* (8), 5057−5086.
(35) Rumyantsev, A. M.; Gavrilov, A. A.; Kramarenko, E. Y. Electrostatically stabilized microphase separation in blends of oppositely charged polyelectrolytes. *Macromolecules* **2019**, *52* (19), 7167−7174.
(36) Zhang, Z.; Huang, C.; Weiss, R.; Chen, Q. Association energy in strongly associative polymers. *J. Rheol.* **2017**, *61* (6), 1199−1207.
(37) Jones, J. E. On the determination of molecular fields.—II. From the equation of state of a gas. *Proc. R. Soc. London, Ser. A* **1924**, *106* (738), 463−477.
(38) Andersen, H. C.; Chandler, D.; Weeks, J. D. Roles of repulsive and attractive forces in liquids: The equilibrium theory of classical fluids. *Adv. Chem. Phys.* **1976**, *34*, 105.
(39) Warner, H. R., Jr Kinetic theory and rheology of dilute suspensions of finitely extendible dumbbells. *Ind. Eng. Chem. Fundam.* **1972**, *11* (3), 379−387.
(40) Meng, D.; Zhang, K.; Kumar, S. K. Size-dependent penetrant diffusion in polymer glasses. *Soft Matter* **2018**, *14* (21), 4226−4230.
(41) Hockney, R. W.; Eastwood, J. W. *Computer simulation using particles*. CRC Press: 2021.
(42) Lee, A. A.; Perez-Martinez, C. S.; Smith, A. M.; Perkin, S. Scaling analysis of the screening length in concentrated electrolytes. *Phys. Rev. Lett.* **2017**, *119* (2), No. 026002.
(43) Eyvazi, N.; Biagooi, M.; Oskoee, S. N. Molecular dynamics investigation of charging process in polyelectrolyte-based supercapacitors. *Sci. Rep.* **2022**, *12* (1), 1098.
(44) Plimpton, S. Fast Parallel Algorithms for Short-Range Molecular Dynamics. *J. Comput. Phys.* **1995**, *117* (1), 1−19.
(45) Allen, M. P.; Tildesley, D. J. *Computer Simulation of Liquids*. Oxford University Press: 2017.
(46) Hoover, W. G. Canonical dynamics: Equilibrium phase-space distributions. *Phys. Rev. A* **1985**, *31* (3), 1695−1697.
(47) Khabaz, F.; Khare, R. Glass transition and molecular mobility in styrene−butadiene rubber modified asphalt. *J. Phys. Chem. B* **2015**, *119* (44), 14261−14269.
(48) Mani, S.; Khabaz, F.; Godbole, R. V.; Hedden, R. C.; Khare, R. Structure and hydrogen bonding of water in polyacrylate gels: effects

https://doi.org/10.1021/acs.macromol.4c00039
Macromolecules XXXX, XXX, XXX−XXX

of polymer hydrophilicity and water concentration. *J. Phys. Chem. B* **2015**, *119* (49), 15381−15393.
(49) Ferry, J. D. *Viscoelastic properties of polymers*. John Wiley & Sons: 1980.
(50) Angell, C. A. Formation of glasses from liquids and biopolymers. *Science* **1995**, *267* (5206), 1924−1935.
(51) Perego, A.; Khabaz, F. Volumetric and rheological properties of vitrimers: a hybrid molecular dynamics and Monte Carlo simulation study. *Macromolecules* **2020**, *53* (19), 8406−8416.
(52) Perego, A.; Lazarenko, D.; Cloitre, M.; Khabaz, F. Microscopic dynamics and viscoelasticity of vitrimers. *Macromolecules* **2022**, *55* (17), 7605−7613.
(53) Montarnal, D.; Capelot, M.; Tournilhac, F.; Leibler, L. Silica-like malleable materials from permanent organic networks. *Science* **2011**, *334* (6058), 965−968.
(54) Röttger, M.; Domenech, T.; van Der Weegen, R.; Breuillac, A.; Nicolaÿ, R.; Leibler, L. High-performance vitrimers from commodity thermoplastics through dioxaborolane metathesis. *Science* **2017**, *356* (6333), 62−65.
(55) Komarov, P. V.; Khalatur, P. G.; Khokhlov, A. R. Large-scale atomistic and quantum-mechanical simulations of a Nafion membrane: Morphology, proton solvation and charge transport. *Beilstein J. Nanotechnol.* **2013**, *4* (1), 567−587.
(56) Theodorou, D. N.; Suter, U. W. Shape of unperturbed linear polymers: polypropylene. *Macromolecules* **1985**, *18* (6), 1206−1214.
(57) Karayiannis, N. C.; Foteinopoulou, K.; Laso, M. The structure of random packings of freely jointed chains of tangent hard spheres. *J. Chem. Phys.* **2009**, *130* (16), No. 164908.
(58) Kob, W.; Donati, C.; Plimpton, S. J.; Poole, P. H.; Glotzer, S. C. Dynamical heterogeneities in a supercooled Lennard-Jones liquid. *Phys. Rev. Lett.* **1997**, *79* (15), 2827.
(59) Pandya, H.; Perego, A.; Khabaz, F. Stress-induced dynamics of glassy vitrimers with fast bond exchange rate. *J. Appl. Polym. Sci.* **2024**, *141* (10), No. e55039.
(60) Chechkin, A. V.; Seno, F.; Metzler, R.; Sokolov, I. M. Brownian yet non-Gaussian diffusion: from superstatistics to subordination of diffusing diffusivities. *Phys. Rev. X* **2017**, *7* (2), No. 021002.
(61) Weiss, R.; Yu, W.-C. Viscoelastic behavior of very lightly sulfonated polystyrene ionomers. *Macromolecules* **2007**, *40* (10), 3640−3643.
(62) Choi, U. H.; Ye, Y.; Salas de la Cruz, D.; Liu, W.; Winey, K. I.; Elabd, Y. A.; Runt, J.; Colby, R. H. Dielectric and viscoelastic responses of imidazolium-based ionomers with different counterions and side chain lengths. *Macromolecules* **2014**, *47* (2), 777−790.
(63) Carden, P.; Ge, S.; Zhao, S.; Li, B.; Samanta, S.; Sokolov, A. P. Influence of molecular architecture on the viscoelastic properties of polymers with phase-separated dynamic bonds. *Macromolecules* **2023**, *56* (13), 5173−5180.
(64) Huang, C.; Chen, Q.; Weiss, R. Nonlinear rheology of random sulfonated polystyrene ionomers: The role of the sol−gel transition. *Macromolecules* **2016**, *49* (23), 9203−9214.

https://doi.org/10.1021/acs.macromol.4c00039
Macromolecules XXXX, XXX, XXX−XXX